

DESIGN OF CREEP-RESISTANT STEELS: SUCCESS & FAILURE OF MODELS

H. K. D. H. Bhadeshia and T. Sourmail

University of Cambridge
Department of Materials Science and Metallurgy
Pembroke Street, Cambridge CB2 3QZ, U.K.

ABSTRACT

The purpose of this paper is to assess the validity of some recent developments in the subject of modelling, in the context of creep deformation and associated topics.

INTRODUCTION

The design of engineering materials generally involves the simultaneous optimisation of large numbers of parameters, often in circumstances where the interactions between the parameters are ill-defined. “Modelling” can lead to the creation of new theory capable of dealing with complexity; the practical goal is to accelerate the design process and to minimise the use of resources. However, the subject has become diffuse and some of the claims being made are unconvincing. It is timely therefore to assess its success, failures and claims. The opportunity to do this in the context of creep-resistant ferritic-steels is particularly exciting, because the goals are high, as are the risks of failure.

It is nice to be able to express science in the language of mathematics. There is satisfaction when the mathematical framework leads to verifiable predictions. This has been the tradition of science over many centuries. What then is special about *modelling*, which after all also relies on a quantitative methodology? We shall begin by attempting to distinguish modelling from ordinary scientific practice. The emphasis of this paper will be on the nature, performance and hidden aspects of models rather than on detail, which has been reviewed recently [1,2].

ORDINARY SCIENCE

One approach in science is to reduce a problem until it can be described rigorously using principles which are well-founded in contemporary knowledge. Taking creep as an example, the focus of this approach has largely been in the steady-state regime, with the creep strain rate for metals is given as a function of the applied stress (σ), the absolute temperature (T) and the grain size (d):

$$\dot{\epsilon} = f\{\sigma, T, d\} \quad (1)$$

or more explicitly as

$$\dot{\epsilon}_{SS} = a_1 \left(\frac{DGb}{kT} \right) \left(\frac{b}{d} \right)^m \left(\frac{\sigma}{G} \right)^n \quad (2)$$

where $\dot{\epsilon}_{SS}$ is the steady-state creep rate, a_1 is usually an empirical constant, D is an appropriate diffusion coefficient, b is the magnitude of the Burgers vector and G is the shear modulus. The stress-exponent n and the grain size exponent m are dependent on the mechanism of creep. When considering particle hardened metals, it is necessary to use an effective stress $(\sigma - \sigma_0)$ where σ_0 is a threshold or friction stress [3]:

$$\dot{\epsilon}_{SS} = a_1 \left(\frac{DGb}{kT} \right) \left(\frac{b}{d} \right)^m \left(\frac{\sigma - \sigma_0}{G} \right)^n \quad (3)$$

Failure to do this can result in artificially large stress-exponents.

Unfortunately, these power-law approaches have never been adequate descriptions of practical materials. They do not account for the many kinds of defects, solutes, time-dependent microstructures *etc.* which are the basis of commercial alloys. To quote Wilshire [4], “for over half a century, reliance on power-law approaches has failed to clarify the mechanisms governing creep strain accumulation . . . , even in pure materials”.

MODELLING

It is necessary to use a different approach capable of dealing with a useful level of complexity, in other words, an approach which does not compromise the problem as originally posed. This is a clear distinction from ordinary science:

Modelling can be defined as a quantitative methodology with emphasis on a *complete* solution which does not compromise the complexity of the original problem.

There are caveats to this definition:

- (a) A model, irrespective of its structure or reliance on empirical knowledge, must be capable of making predictions which are *verifiable*.
- (b) Any predictions should be associated with indications of uncertainty. The first sort of uncertainty is called *noise*, which arises because some variables may not be controlled in experiments which are repeated. The second kind is the uncertainty of the structure of the model itself.
- (c) The structure of the model must be such as to give insight into the physics behind the problem being modelled.

Fig. 1 illustrates the difference between the ordinary method and the one adapted for complexity. In modelling there is no shame in combining the basic principles of science with empiricism in order to avoid simplification. There is a clear treatment of uncertainties. The result will not be as transparent as ordinary science so it is important for the model to be *used* as widely as possible. This is to allow the model to be exposed to independent scrutiny and exposure to unforeseen circumstances.

A complicated model cannot be considered to be validated until it has been tested and interrogated over a range of circumstances. One way to achieve this is to make the model available to the wider scientific community.

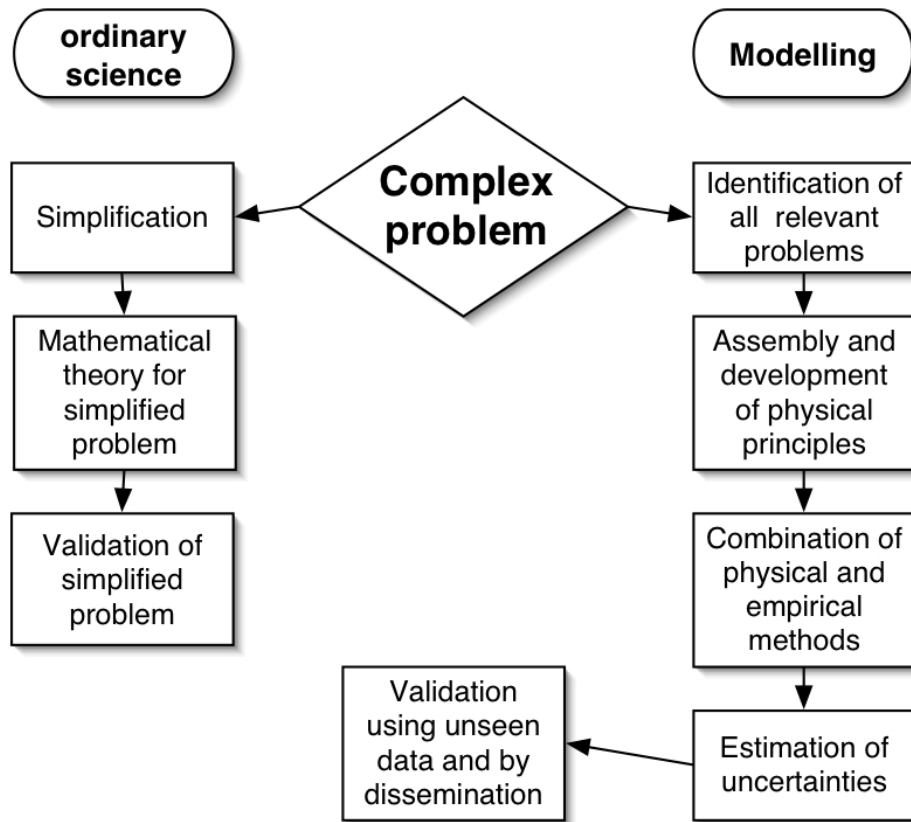


Fig. 1: An illustration of the difference between ordinary scientific method and modelling as defined here. The feedback between these two methods, and the timescales, are not illustrated for the sake of clarity.

FITTING PARAMETERS

A fitting parameter is like a proportionality factor whose physical meaning is not clear. With the plethora of modelling techniques now available, unjustified claims are frequently made about the physical significance of the method and how it avoids fitting parameters. It is worth illustrating this with a couple of examples which are deliberately chosen to be outside the field of creep deformation in order to retain the attention of the reader.

Phase Field Models

One example is the recent claim that the phase-field method involves no curve fitting, and hence is the best method for modelling weld microstructures [5]. A phase-field method describes the entire microstructure, including the interface, in terms of a variables known as the *order parameters*. The precipitate and matrix each have a particular value of the order parameter. Likewise, the interface is located by the position where the order parameter changes from its precipitate-value to its matrix-value. The order parameter is thus continuous on traversing

the precipitate and entering the matrix (Fig. 2). The range over which it changes is the width of the interface. The set of values of the order parameter over the whole microstructure is the *phase field*.

A theory which tracks the dynamics of the order parameter across the entire phase field, would allow the evolution of the microstructure to be calculated without the need to track the interface. Such a theory would require the free energy as a function of the order parameter so that the field can follow a path which leads to a maximisation of entropy production.

The free energy per atom of an inhomogeneous solution is then given by:

$$g_{ih} = \int \left[g\{c_0\} + v^3 \kappa (\nabla c)^2 \right] dV \quad (4)$$

where $g\{c\}$ is the free energy per atom in a homogeneous solution of concentration c_0 , v is the volume per atom and κ is called the *gradient energy coefficient*. g_{ih} is often referred to as a free energy *functional* since as in density functional theory, it is a function of a function. *****CALPHAD paper

In phase field theory as applied to the modelling of microstructure, the gradient energy coefficient is a fitting parameter. If strain as well as composition are included in the analysis then at least two such coefficients have to be fitted. The number density of particles is sometimes included in the method simply by arbitrarily including a site density from which particles grow from time zero. This again is fitting. It is false therefore to claim [5] that the method does not involve fitting parameters.

“Smart” Models

Kumar *et al.* [6] have coined the term “Smart Model” in attempting to get a precise description of the shape of a weld pool. Their work is based on the equations of heat and fluid flow. However, it is found that whereas the physics captures the essence of the weld pool, the agreement with experimental observations is not adequate in the context of industrial requirements. To cope with this they essentially use a non-linear regression method, constrained by the physical equations, to make certain parameters such as viscosity, empirical variables whose values are determined by fitting to experimental data. It is claimed that this is a better approach than neural networks or inverse modelling, but neural networks can incorporate physical equations to constrain the fitting component [7].

Summary

Each modelling technique has advantages and disadvantages and when dealing with complex problems, they all have fitting parameters. The focus should not be on the fitting parameters, but rather on whether the model makes useful predictions and gives insight into the mechanisms involved. Furthermore, a good model must indicate uncertainty when extrapolating out of its domain of training.

There are no creep models which are free of fitting parameters. The test of a good model is its ability to generalise without unwittingly exposing the user to the dangers of extrapolation.

MICROSTRUCTURE MODELS

Yin and Faulkner have used classical nucleation and growth theory to simulate the precipitation of $M_{23}C_6$ in a particular power plant steel [8]. The fitting parameters in their nucleation model include the number density of nucleation sites and the carbide–ferrite interfacial energy per unit area. The theory also incorporates the following approximations, that multicomponent diffusion can be neglected (*i.e.* the growth theory only accounts for chromium diffusion), that the mean–field approximation to the distribution of solute applies, that capillarity effects can be calculated without allowing for multicomponent effects, *etc.*

One of their graphs is illustrated in Fig. 3 where an “equivalent radius” is compared against experimental data. Notice that the experimental data are for the stage of tempering where coarsening dominates. Such data do not represent a good test of the kinetic assumptions since it is the early part of the precipitation curve that is sensitive to nucleation and growth phenomena. Indeed, the radius beyond about 10 h on the graph, whence the $M_{23}C_6$ has almost reached its equilibrium fraction, depends strongly on the fitting parameters used in the nucleation function. Not only is the model weakly validated, but it has also not been used to make predictions of independent data, or predictions which can later be verified. One cannot therefore be certain about the ability of the model to generalise. More rigorous models have been reviewed [2] and will be discussed later in this section.

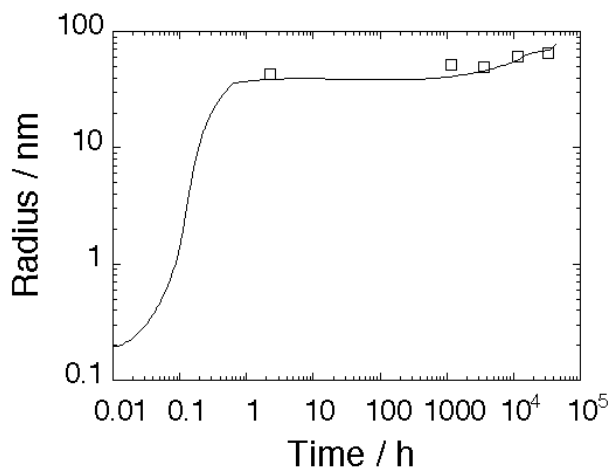


Fig. 3: The “equivalent circle radius” of $M_{23}C_6$ particles plotted as a function of time at 650°C . After Yin *et al.*

Coarsening Theory

Consider a particulate phase θ in a ferritic matrix α . The solute concentration in the ferrite is written $c^{\alpha\theta}$ and that in θ written $c^{\theta\alpha}$ assuming that the two phases are in equilibrium at a flat interface. However, if the interface is curved, for example when the particles are in the form of spheres, the equilibrium concentrations become a function of the radius of curvature, given by $c_r^{\alpha\theta}$ and $c_r^{\theta\alpha}$ respectively, where r is the particle radius. This is the Gibbs–Thompson capillarity effect. It accounts for the cost of creating interface as the particle grows.

It can be shown that the concentration $c_r^{\alpha\theta} > c^{\alpha\theta}$, the inequality becoming larger as $r \rightarrow 0$. In other words, the solute concentration in the ferrite near a small particle will be greater than

that in contact with a large particle, thus setting up a concentration gradient which makes the small particle dissolve and the larger particle grow (Fig. 4). This is the process of coarsening, driven by the interfacial energy σ .

The concentration difference $c_r^{\alpha\theta} - c^{\alpha\theta}$ which drives the diffusion flux is given by

$$c_r^{\alpha\theta} - c^{\alpha\theta} = \frac{\sigma V^\alpha}{kT r} \times \frac{c^{\alpha\theta}(1 - c^{\alpha\theta})}{c^{\theta\alpha} - c^{\alpha\theta}} \quad (5)$$

where k is the Boltzmann constant, T the absolute temperature and V^α the molar volume of the ferrite. This flux feeds the growth or dissolution of the particle and hence must match the rate at which solute is absorbed or desorbed at the moving interface:

$$\underbrace{D(c_r^{\alpha\theta} - c^{\alpha\theta})}_{\text{measure of flux}} \propto \underbrace{v(c^{\theta\alpha} - c^{\alpha\theta})}_{\text{rate of solute absorption}}$$

where v is the interfacial velocity and D is the solute diffusivity in the matrix phase. On substituting for the concentration difference and using Fick's first law, it follows that

$$v \propto D \frac{\sigma V^\alpha}{kT r} \times \underbrace{\frac{c^{\alpha\theta}(1 - c^{\alpha\theta})}{(c^{\theta\alpha} - c^{\alpha\theta})^2}}_{\text{instability}} \quad (6)$$

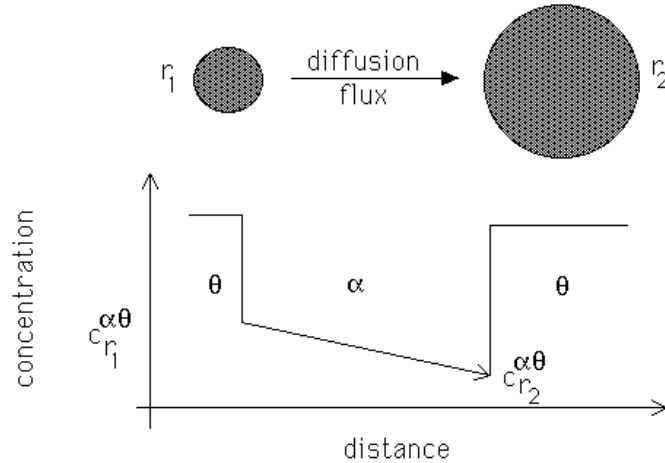


Fig. 4: An illustration of the capillarity effect driving coarsening.

In equation 6, the equilibrium concentration term on the right is a thermodynamic term, a larger value of which corresponds to a greater coarsening rate. Fig. 5 shows the equilibrium chromium concentrations in the ferrite and $M_{23}C_6$ phases for a large variety of power plant steels. The concentrations are clearly largest for the more modern martensitic alloys which are Cr-rich; such steels are designed for higher temperature service and hence require a greater

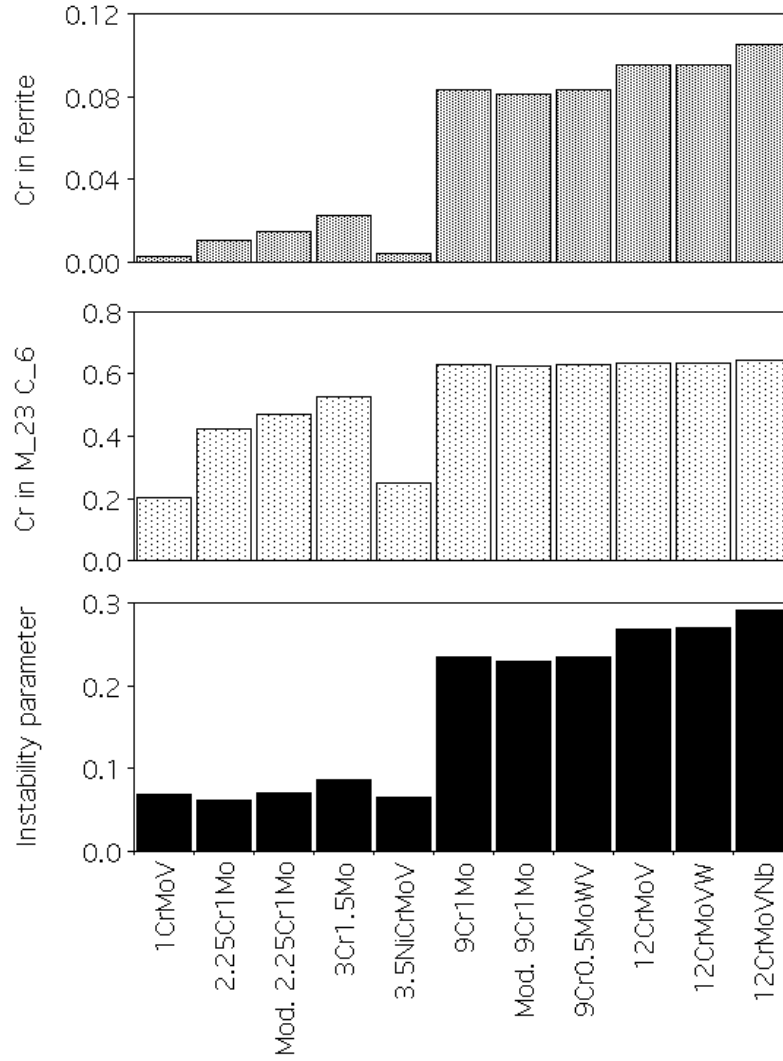


Fig. 5: The top two bar charts give the chromium concentrations (mole fractions) in ferrite and in $M_{23}C_6$ respectively. The actual compositions of the steels are given in [9]. The third bar chart is gives a measure of the tendency for $M_{23}C_6$ to coarsen assuming equation 6.

oxidation resistance. It is evident, however, that the tendency for $M_{23}C_6$ to coarsen should be greatest in the Cr-rich alloys.

Commercial steels contain many solutes whereas equation 6 deals with just one. Venugopalan and Kirkaldy [10] generalised the theory to deal with many solutes, assuming that the effects of the different fluxes could be combined into a single, effective diffusion coefficient D_{eff} by treating the fluxes as a combination of parallel electrical conductances. Equation 6 can be rearranged as follows:

$$\frac{1}{v} \propto \frac{1}{D_i} \times \frac{(c_i^{\theta\alpha} - c_i^{\alpha\theta})^2}{c_i^{\alpha\theta}(1 - c_i^{\alpha\theta})}$$

where i now represents a particular solute. In a multicomponent alloy, the right hand side is

replaced by a summation

$$\frac{1}{v} \propto \frac{1}{D_{eff}} \quad \text{where} \quad \frac{1}{D_{eff}} = \sum_i \frac{1}{D_i} \times \frac{(c_i^{\theta\alpha} - c_i^{\alpha\theta})^2}{c_i^{\alpha\theta}(1 - c_C^{\alpha\theta})} \quad (7)$$

This multicomponent treatment does not in fact make a difference to the ranking of the $M_{23}C_6$ coarsening tendency as presented in Fig. 5, because this carbide is chromium-rich and because the diffusivities of the substitutional solutes are not very different.

Coarsening in Multiphase Microstructures

Abe [11] has reported interesting data on the coarsening of $M_{23}C_6$ particles in Fe-9Cr-W steels as a function of the tungsten content and of time during creep testing at 600 °C (Fig. 6a). According to Abe, the addition of tungsten reduces the coarsening rate. The data have to be interpreted with care because the addition of tungsten also causes the precipitation of Laves phase (Fig. 6b), but the fact that the data are from creep test samples should not matter since it is the trend as a function of W that we are interested in; we shall also assume that the electron microscopy data refer strictly to $M_{23}C_6$ and do not unintentionally include any other phases. Fig. 6c shows two sets of calculated values of D_{eff} , one assuming that it is only the diffusion of chromium (the major constituent of $M_{23}C_6$ in such alloys) that controls coarsening, and the other using the multicomponent formalism (equation 7). As stated earlier, the trends are identical for the two sets of calculations, but in contradiction to the experimental data, they all suggest that the addition of tungsten should *accelerate* the rate at which $M_{23}C_6$ coarsens. The calculations show also that the experimental data cannot be explained by saying that tungsten reduces the overall diffusion coefficient [11].

A possible explanation is that Laves phase precipitates some time after $M_{23}C_6$, in which case it may be appropriate to consider a constrained equilibrium in which Laves phase is excluded. In fact, when this is done, M_6C is promoted and the situation worsens in the sense that D_{eff} for $M_{23}C_6$ is predicted to increase.

How the addition of tungsten reduces the coarsening of $M_{23}C_6$ can be explained by taking into account all of the phases that are present. When there is more than one precipitate phase in the microstructure, differences in interfacial energy (σ , equation 7) cannot be neglected. Laves phase has a higher interfacial energy so the concentration in ferrite in equilibrium with Laves will, for the same particle radius, be higher for Laves than for $M_{23}C_6$:

$$c_{r,Laves}^{\alpha\theta} > c_{r,M_{23}C_6}^{\alpha\theta}$$

This is illustrated schematically in Fig. 6d on a concentration-distance plot. In addition to a flux of solute from small Laves phase particles to larger ones, there will also be a flux to both small and large $M_{23}C_6$ particles. The coarsening rate of $M_{23}C_6$ will therefore be reduced whereas that of Laves phase accelerated. It is interesting that Abe specifically commented that the coarsening rate of Laves phase was extremely rapid.

Coarsening kinetics do not in fact require an explicit treatment but follow naturally from the precipitation theory which for each phase includes the capillarity effect. Indeed, it is well known that the separation of precipitation and coarsening is artificial, because capillarity makes the smaller precipitates grow at a slower rate than those which nucleated first and hence are larger, even before the equilibrium fraction is reached [12,13]. Fig. 7 shows the results of calculations of this kind, the mean particle radius at first increasing approximately parabolically with time as all particles grow from solid solution. The mean radius then changes as about $t^{\frac{1}{3}}$ at longer

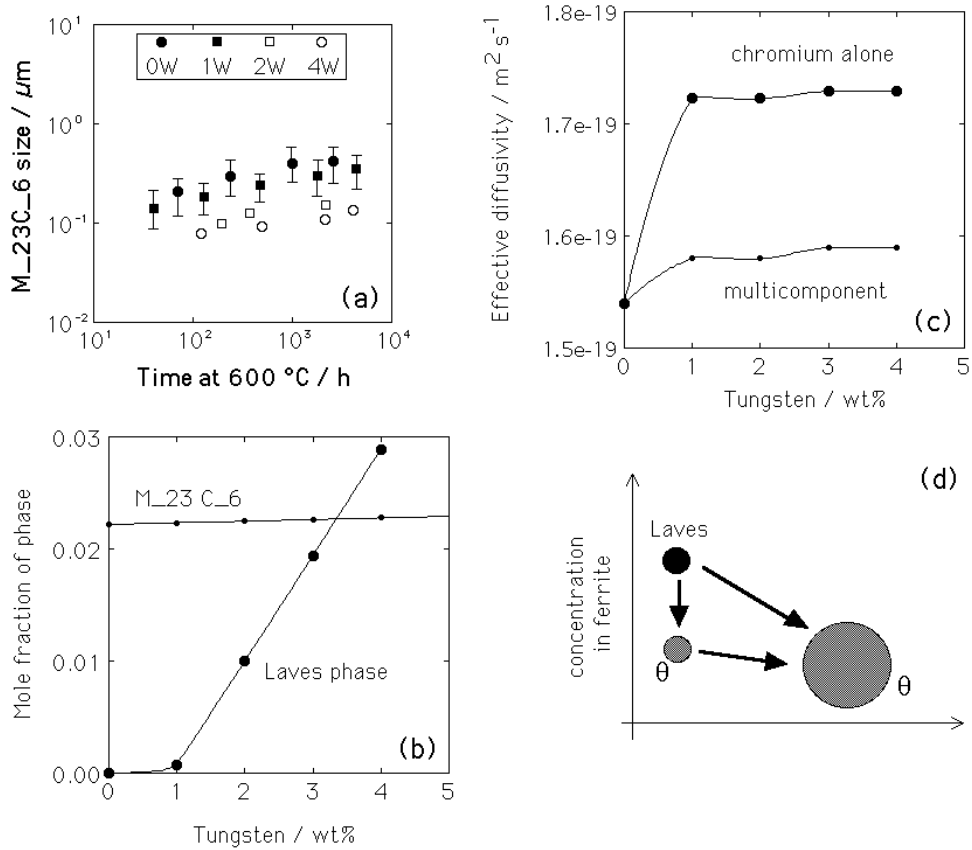


Fig. 6: Coarsening data from Fe-0.1C-9Cr-0.5Mn-0.3Si wt% steel, containing a variety of tungsten additions, tested in creep at $600\text{ }^\circ\text{C}$ [11]. (a) $M_{23}C_6$ size. The error bars have been omitted for the highest W data for clarity. (b) Equilibrium phase fraction calculations for $600\text{ }^\circ\text{C}$ carried out using MTDATA with the SGTE database, allowing all common carbides and Laves phase and Fe, C, Cr, Mn, Si, W as the components. (c) Values of D_{eff} for $M_{23}C_6$, for two cases, the first where chromium alone is considered and then for multicomponent diffusion. (d) Schematic illustration of why the presence of Laves phase retards the coarsening of $M_{23}C_6$.

times as the number density of particles decreases, consistent with expectations from coarsening theory. It is important to emphasise that there is no separate treatment of precipitation and coarsening here, both are in an inclusive theory.

Whereas multicomponent effects can already be taken into account in coarsening theory, there is not yet a proven theory to cover multiphase coarsening.

To illustrate the level of agreement that has been achieved between precipitation and coarsening theory and experimental data, Fig. 8 shows a variety of comparisons for molybdenum

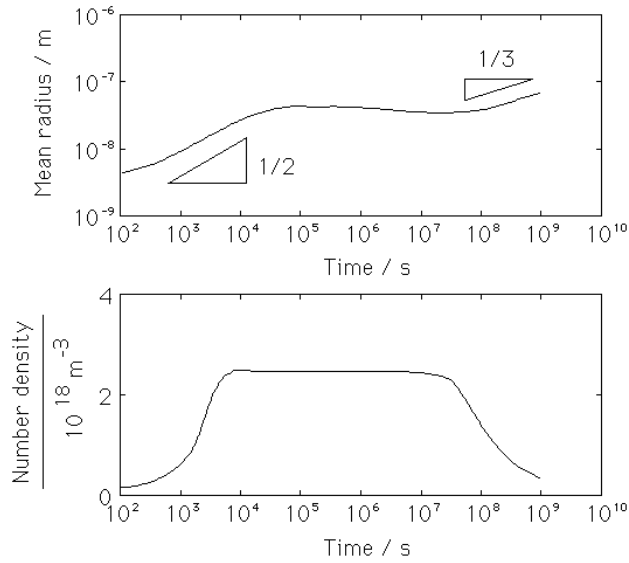


Fig. 7: The precipitation and coarsening of niobium carbide precipitates in austenite [13] in Fe–0.05Nb–0.1C wt% steel, beginning with a supersaturated solid solution at 900 °C. The number density of nucleation sites was taken to be $9 \times 10^{19} \text{ m}^{-3}$, with $\sigma = 0.26 \text{ J m}^{-2}$. [13]

carbide in ferrite [12]. The only fitting–parameters used are the interfacial energy per unit area and the number density of nucleation sites, but the treatment is otherwise multicomponent and in a simultaneous transformations framework [14,15] which avoids assumptions about the dissolution of cementite during the precipitation of the alloy carbide. Notice that the method has been demonstrated to be capable of including precipitation at a variety of sites, for example, grain boundary and intragranular precipitation [16].

Recent Coarsening Theory

Yin and Faulkner [17] recently theorised about the effect of alloying elements on the coarsening behaviour of M_{23}C_6 precipitates in ferritic power–plant steels. The essence of their theory is that any solute which reduces the solubility of chromium in ferrite also reduces the coarsening rate. It is argued that one effect of the reduction is to enhance the nucleation rate and hence a lead to a finer initial size–distribution.

It is difficult to have confidence in this model because it contains a number of premises, the most important of which is that the formation of M_{23}C_6 is treated as a binary Fe–Cr problem in the kinetic theory. The equations for diffusion–controlled growth therefore feature only the terms associated with chromium. This is known to be a poor approximation because in ternary or higher–order steels, the presence of fast–diffusing carbon alters the tie–line governing interface compositions during diffusion–controlled growth. A brief explanation of this phenomenon, first treated quantitatively by Coates [18,19,20,21], is as follows.

For isothermal transformation in a binary alloy, the concentrations at the interface between the parent γ and precipitate α are given by a tie–lie of the phase diagram. The diffusion flux of solute from the interface must equal the rate at which solute is incorporated in the precipitate

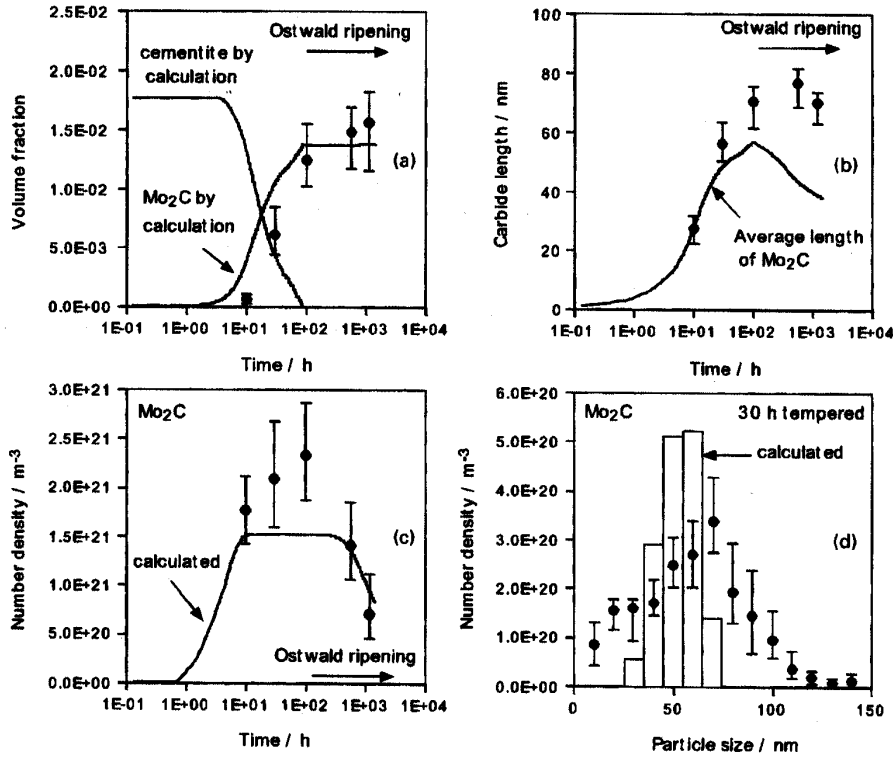


Fig. 8: Kinetics of molybdenum carbide formation in tempered martensite.

so that:

$$\underbrace{(c^{\gamma\alpha} - c^{\alpha\gamma}) \frac{\partial z^*}{\partial t}}_{\text{rate solute partitioned}} = \underbrace{-D \frac{\partial c}{\partial z}}_{\text{diffusion flux from interface}} \quad (8)$$

where z is a coordinate normal to the interface with a value z^* at the position of the interface. Note that the concentration gradient is evaluated at the position of the interface ($z = z^*$). $c^{\gamma\alpha}$ is the solubility of solute in γ which is in equilibrium with α and similarly, $c^{\alpha\gamma}$ is the corresponding solubility in α which is in equilibrium with γ .

In a ternary steel, it would be necessary to satisfy two equations of the form of equation 8, simultaneously, for each of the solutes (identified by the subscript on c , with c_1 representing carbon and c_2 the substitutional solute):

$$\left. \begin{aligned} (c_1^{\gamma\alpha} - c_1^{\alpha\gamma})v &= -D_1 \nabla c_1 \\ (c_2^{\gamma\alpha} - c_2^{\alpha\gamma})v &= -D_2 \nabla c_2 \end{aligned} \right\}$$

The interface velocity v is the $\partial z^*/\partial t$ in equation 8.

Because $D_1 \gg D_2$, these equations cannot in general be simultaneously satisfied for the tie-line passing through the alloy composition \bar{c}_1, \bar{c}_2 . It is, however, possible to choose other tie-lines which satisfy both equations. This in general has a great effect on growth kinetics, a factor absent from the theory of Yin and Faulkner.

Unfortunately, their treatment neglects a number of other effects that are associated with steels which are not binary, particularly with respect to capillarity and diffusion phenomena. Their

equations 8 and 9 imply that different volume fractions are obtained depending on which solute is used to calculate the fraction. The volume fraction must be independent of the solute; the problem arises because of the failure to use different rules to determine the volume fraction in higher order systems (see for example, the use of tie-triangles in reference 22).

They use vertical sections of ternary phase diagrams (their Figs. 5–7) to illustrate changes in solubility, whereas in fact the tie-lines do not necessarily lie in the plane of those diagrams.

It is worth noting that the model has not been experimentally verified other than two points in their Fig. 2, whose positions depend on the fitting parameters used in the nucleation and growth functions. The model does not reproduce the observations of Abe as described earlier [11].

PARAMETRIC MODELS

We have emphasised that practical creep-resistant materials are complex and hence cannot be adequately designed using the creep mechanisms described at the beginning of this paper. It is nevertheless important to know the long-term creep and rupture behaviour of such materials for their safe use in safety-critical applications such as power plant and aeroengines. For this reason there exist a large number of empirical or semi-empirical methods, which permit the accurate representation of experimental data and at the same time facilitate the extrapolation of short-term creep data, to varying degrees of success. Many of these methods have been reviewed recently [1,23]. The following sections describe a few of the methods in order to highlight developments in the subject.

Creep strain is a direct measure of remaining life so the safe extrapolation of short-term creep data is a major goal of structural integrity assessment. A popular method involves the use of a θ -parameter equation [24] :

$$\epsilon = \underbrace{\theta_1 [1 - \exp\{-\theta_2 t\}]}_{\text{decaying rate}} + \underbrace{\theta_3 [\exp\{\theta_4 t\} - 1]}_{\text{accelerating rate}} \quad (9)$$

where θ_i are obtained by fitting to experimental data, and t is the time at temperature. The first two of these parameters describe the primary or decaying strain rate component, whereas the remaining terms the accelerating regime.

The steady-state creep theory described earlier leads to an equation of the form

$$\dot{\epsilon} = a_3 \sigma^n \exp\left\{-\frac{Q}{RT}\right\} \quad (10)$$

where a_3 is an empirical constant. This can be integrated to find the creep rupture time t_r as

$$\ln\{t_r\} = \ln\left\{\frac{\epsilon_r}{a_3}\right\} - n \ln\{\sigma\} + \frac{Q}{RT} \quad (11)$$

Nevertheless, it is found in practice that slightly better fits are obtained by writing [25,26,27]

$$\ln\{t_r\} = a_4 + a_5 \sigma + a_6 T \quad (12)$$

where a_i , are fitting constants.

Whilst parametric models like these have been widely and successfully applied, they simply are not sufficiently general to deal with large numbers of variables. A more modern technique

is the neural network method which thrives in complexity. The method has now been demonstrated to be superior in the extrapolation and representation of creep data. Indeed, we would strongly suggest that the neural network method (Bayesian framework) would be a better way of treating creep data with the aim of developing product and design standards than the techniques currently adopted, for example by the European Creep Collaborative Committee [28].

NEURAL NETWORK MODELS

A general method of non-linear regression which avoids the difficulties described above is neural network analysis, as described elsewhere [1]. The details are not discussed here, suffice it to say that there are well-established procedures to avoid overfitting and to give excellent estimates of noise and indeed the uncertainty of creating the model in regions of the input space where data are sparse, noisy or absent. The danger of extrapolation is reduced by a nice treatment of uncertainties.

The neural network can capture interactions between the inputs because it is nonlinear. It can be interrogated to make predictions and to see how these depend on various combinations of inputs.

This methodology has proved to be extremely useful in the analysis of creep phenomena and in structural integrity assessment. The application and success of neural networks in creep have recently been assessed and reviewed [1,2], with many examples where the number of variables is greater than 50. We shall now illustrate this with an example on steels.

Influence of Microstructure

Although the link between microstructure and the creep properties is well-understood for simple systems, the relative importance of the roles of precipitates, solid solution strengthening, microstructure *etc.* in determining the long-term creep rupture properties have not been revealed in the context of applicable alloys.

The neural network method, combined with phase stability calculations, has recently been used to accomplish a non-linear factorisation of the creep-rupture strength into individual components as illustrated in Fig. 9 [29]. It is clear, for example, that the proportion of the contribution to the 10^5 h creep-rupture strength from dissolved solutes increases at 600°C when compared with its role at 500°C . The method is now being used to design microstructures and alloys for their long-term properties. Similar methods have been applied to the nickel-base superalloys.

The NIMS Contribution

The National Institute of Materials Science (NIMS) in Japan does an impressive job of measuring and archiving creep data for a large range of materials. These data are made freely available and hence represent a rich source of valuable information. Using these and other published data, Sourmail *et al.* created a comprehensive neural network model for the creep rupture strength of austenitic stainless steels, as a function of the chemical composition (16 different elements), the solution treatment temperature, test temperature and time [30]. Much work was carried out to validate the model and to examine its behaviour. However, confidence was boosted when new, long-term creep data were published by NIMS, data which were not included in the creation of the model [*cf.* reference 31 and 32].

Fig. 11 illustrates predictions and experimental data (points) for 18Cr-12Ni-Nb austenitic stainless steels [32]. The shaded regions are obtained using the neural network model, the

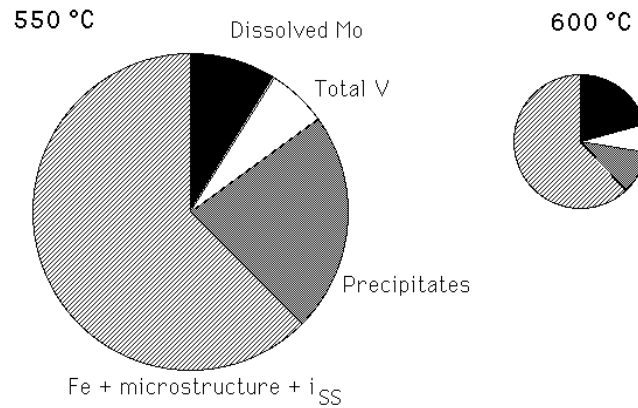


Fig. 10: Factorisation of the 10^5 h creep-rupture strength of a $2\frac{1}{2}\text{Cr1Mo}$ steel at the appropriate temperature. The term i_{SS} represents solid solution strengthening due to elements other than Mo or V. The diameter of each of the pie-charts scales with the creep rupture strength which is 79 and 30 MPa for 550°C and 600°C respectively. (Muruganath and Bhadeshia, 2002).

width of the shaded region representing the $\pm 1\sigma$ uncertainties. The curve represents the NIMS prediction using the Orr-Sherby-Dorn method in which the creep rupture data are fitted to an empirical time-temperature parameter using 5th order polynomials. The constant standard error in $\log\{t\}$ was stated to be about 0.102 for steel AEA and 0.154 for steel AEG (t is the time in hours). In the neural network prediction, the uncertainty is not constant but varies depending on where in the input domain the calculations are done. It is clear that the neural network makes better predictions of the unseen long-term data, a fact that is not surprising given that it represents the most general empirical approach.

The neural network and other models associated with creep deformation are freely available from Cambridge University on www.msm.cam.ac.uk/phase-trans

We urge people to use these and test their validity in the broadest sense. Calculations can even be conducted on-line.

CONCLUSIONS

We have in this paper tried to illustrate the state of modelling methods in the context of creep deformation. Particular emphasis has been placed on dispelling the myth that anything with fitting parameters is bad and that there are methods capable of dealing with complexity which do not involve fitting parameters. We hope that this review encourages a better assessment and dissemination of models.

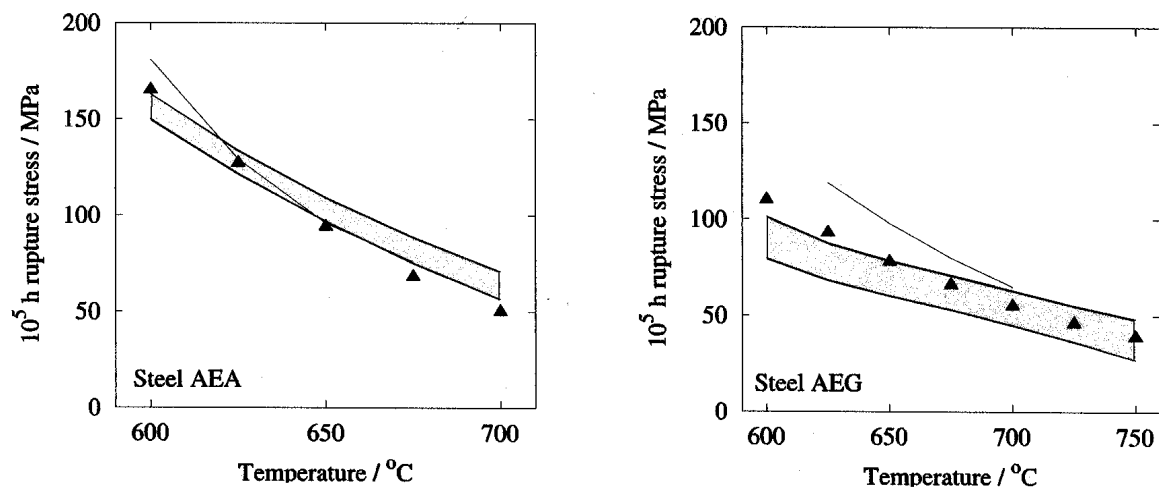


Fig. 11: The shaded regions represent neural network model predictions, the curves the NIMS predictions made using the Orr–Sherby–Dorn method. The experimental data were revealed for the two stainless steels after the predictions were made.

ACKNOWLEDGMENTS

Professor Bhadeshia is extremely grateful to the Japan Society for the Promotion of Science for financing his participation in the meeting held at the Tokyo Institute of Technology, via the good offices of Dr Abe of NIMS.

REFERENCES

1. H. K. D. H. Bhadeshia: *ISIJ International* **39** (1999) 966–979.
2. H. K. D. H. Bhadeshia: *ISIJ International* **41** (2001) 626–640.
3. T. G. Langdon: *Dislocations and creep, Dislocations and Properties of Real Materials*, Institute of Metals, London (1985) 221–238.
4. B. Wilshire: *Strength, Fracture and Complexity* **1** (2003) 39–46.
5. R. G. Thiessen: *Mathematical Modelling of Weld Phenomena 7*, published by T.U. Graz, Austria (2003) in press.
6. A. Kumar, W. Zhang, C.-H. Kim and T. DebRoy: *Mathematical Modelling of Weld Phenomena 7*, published by T.U. Graz, Austria (2003) in press.
7. M. A. Yescas–Gonzalez, H. K. D. H. Bhadeshia and D. J. C. MacKay: *Materials Science and Engineering A* **311** (2001) 162–173.
8. Y. F. Yin and R. G. Faulkner: *6th International Charles Parsons Turbine Conference, Engineering Issues in Turbine Machinery, Power Plant and Renewables*, eds A. Strang, R. D. Conroy, W. M. Banks, M. Blackler, J. Leggett, G. M. McColvin, S. Simpson, M. Smith, F. Starr and R. W. Vanstone, Institute of Materials, London (2003) 525–535.
9. H. K. D. H. Bhadeshia, A. Strang and D. J. Gooch: *International Materials Reviews* **43** (1998) 45–69.
10. D. Venugopalan and J. S. Kirkaldy: *Hardenability Concepts with Applications to Steels*, eds D. V. Doane and J. S. Kirkaldy, TMS–AIME, Warrendale, Pennsylvania, USA

- (1978) 249–267.
11. F. Abe: *Fourth International Conference on Recrystallisation and Related Phenomena*, eds T. Sakai and H. G. Suzuki, The Japan Institute of Metals (1999) 289–294.
 12. S. Yamasaki and H. K. D. H. Bhadeshia: *Materials Science and Technology* **19** (2003) 723–731.
 13. N. Fujita and H. K. D. H. Bhadeshia: *Materials Science and Technology* **17** (2001) 403–408.
 14. J. D. Robson and H. K. D. H. Bhadeshia: *Materials Science and Technology* **13** (1997) 631–639.
 15. S. J. Jones and H. K. D. H. Bhadeshia: *Acta Materialia* **45** (1997) 2911–2920.
 16. S. J. Jones and H. K. D. H. Bhadeshia: *Metallurgical and Materials Transactions A* **28A** (1997) 2005–2013.
 17. Y. F. Yin and R. G. Faulkner: *Materials Science and Engineering A* **A344** (2003) 92–102.
 18. D. E. Coates: *Metallurgical Transactions* **3** (1972) 1203–1212.
 19. D. E. Coates: *Metallurgical Transactions* **4** (1973) 395–396.
 20. D. E. Coates: *Metallurgical Transactions* **4** (1973) 1077.
 21. H. K. D. H. Bhadeshia: *Progress in Materials Science* **29** (1985) 321–386.
 22. D. R. F. West and N. Saunders: *Ternary Phase Diagrams in Materials Science*, 3rd edition, Institute of Materials, London (2002)
 23. M. Evans: *Materials Science and Technology* **15** (1999) 647–658.
 24. R. W. Evans and B. Wilshire: *Creep of Metals and Alloys*, The Institute of Metals, London (1985)
 25. B. J. Cane: *Metal Science*, **13** (1981) 287–294.
 26. S. M. Beech, D. J. Gooch and A. Strang: *Third International Charles Parsons Conference on Materials Engineering in Turbines and Compressors*, Newcastle-upon-Tyne, U. K. (1995) 277–291.
 27. R. W. Evans and B. Wilshire: *Creep of Metals and Alloys*, The Institute of Metals, London (1985)
 28. S. R. Holdsworth and G. Merckling: *6th International Charles Parsons Turbine Conference, Engineering Issues in Turbine Machinery, Power Plant and Renewables*, eds A. Strang, R. D. Conroy, W. M. Banks, M. Blackler, J. Leggett, G. M. McColvin, S. Simpson, M. Smith, F. Starr and R. W. Vanstone, Institute of Materials, London (2003) 411–426.
 29. M. Muruganath and H. K. D. H. Bhadeshia: *Mathematical Modelling of Weld Phenomena 6*, eds H. Cerjak and H. K. D. H. Bhadeshia, Maney Publishers, London (2002) 243–260.
 30. T. Sourmail, H. K. D. H. Bhadeshia and D. J. C. MacKay: *Materials Science and Technology* **18** (2002) 655–663.
 31. NIMS: *Creep Data Sheet 28A*, 18Cr–12Ni–Nb Stainless Steel (1983) 1–12.
 32. NIMS: *Creep Data Sheet 28B*, 18Cr–12Ni–Nb Stainless Steel (2001) 1–25.